Introduction

For ten years, optical telecommunications have had spectacular success, thanks to the explosion of the Internet. This spectacular development is the fruit of a great research and development effort in the field of guided optics, which led to the improvement of the performances of optical fibers. Appearing at the same time was the need to develop optical and optoelectronic components with a planar technology, able to generate, detect, modulate or commutate light, using waveguiding structures. This field of investigation is called integrated optics.

The research and developments undertaken in these two fields (guided and integrated optics) made it possible to provide on the market, optoelectronic components of any kind at low cost. Consequently, other applications in various fields were also developed.

As a matter of fact, today the use of optics includes strategic fields like space, military fields and also fields in everyday life like data storage (CD and DVD), medicine and unsuspected sectors like the car industry.

In a competitive way, the advent of nano-photonics is pushing the limits of photonic system miniaturization to scales lower than the wavelength. Ultimately, the 20^{th} century was the century of electronics, and the 21^{st} century will probably be the century of photonics. The basic idea supporting the use of the photon rather than the electron comes from the very high optical frequencies (200 THz), which allow a very broad bandwidth and offer an unequaled data transmission capacity.

Although optics is a very old science, its major improvements were made during the last quarter of the century. The first work on optics is from the School of Alexandria, Euclid (325-265 BC). However, the reform of optics was undertaken by the Muslim scientists of the medieval period with, at their head Al-Kindi (801-873) and especially Ibn Al-Haytham known under the name of Alhazen (965-1040). This

famous scientist truly created the foundation of modern optics with his experimental approach to the propagation of light. He, indeed, introduced experimentation into physics and provided the basis for understanding the luminous phenomena and the control of light propagation (reflection and refraction).

The heritage of this eminent scientist was transmitted to us through his major book "Kitab Al-Manazir" (*The Book of Vision*) which was translated into Latin and distributed throughout western countries at the beginning of the 13th century. This book was used as a reference until the 17th century and influenced work on optics of the majority of renaissance period scientists. The first philosopher who studied and diffused Ibn Al-Hyatham's work was his enthusiastic disciple Roger Bacon (1214-1292). He was aware of the importance of the Muslim heritage in the fields of science and philosophy. The science historian Gerard SIMON wrote:

> *Roger Bacon was the first to know the Optics of Alhazen (Ibn Al-Haytham) very well... he contributed to its diffusion and he particularly built on it his own work on optics, the Perspective and Multiplication Specierum* (towards 1260-1265)*... he thus accurately followed the analysis of the role of light, the description of the eye, theory of perception and the study of reflection and refraction formulated by Alhazen*. [Adding:] *Kepler renews optics (Paralipomena AD Vitellionem) around 1604 thanks to reading Alhazen and Witelo*.

D.C. Lindgerg emphasizes that Roger Bacon and Johannes Kepler were without any doubt the best disciples of Alhazen (*Optics & Photonics News*, 35 (2003)).

If the revolution of the concepts relating to light sometimes took several centuries, the explosion of telecommunications in the 1980s allowed optics to become a major technology in our everyday life.

Over the last few decades, the approach based on fundamental research and the development of new concepts has been transformed into research and development for new optical products in order to fulfill the increased demand of integrated optoelectronic components in particular for optical telecommunications.

Thus, optics have progressed and moved through four generations: conventional optics, micro-optics, integrated optics and more recently nano-optics (nano-photonics). From optical components of laboratory dimensions (meter and centimeter), research was directed towards micro-optics, particularly with the advent of optical fiber and laser diodes which made it possible to miniaturize photonic systems. Thereafter, integrated optics introduced the concept of integrated optical circuits by similarity to the integrated circuits in micro-electronics. This technology

made it possible in many cases to be released from the limitations imposed by the use of light for signal processing.

The concept of "integrated optics" was introduced for the first time by S.E. Miller in 1960 from Bell Laboratories (USA). The approach suggested by Miller consisted of creating on the same substrate, passive and active components for light generation and treatment. The basic element of this type of circuit is the waveguide.

Finally, in the continuity of the idea suggested for the first time by the physicist R. Feynman in 1959, who spoke about the concept "Smaller, Faster, Cheaper", for which the emergent idea was the possibility of handling matter on an atomic and molecular scale in order to conceive and produce sub-micrometric components and systems, there thus appeared the concept of nanotechnology, which became a new challenge for scientific research around the world. In this nano-scale world, the photon is also building its own realm. Thus, nano-photonics actually make it possible to develop new optical components for light generation and treatment based on new paradigms (such as photonic crystals).

Progress in the previously mentioned research fields is incontestably determined by the fabrication and characterization of structures making it possible to manipulate the photon. Among them is the optical waveguide which constitutes the basic element of any integrated optical circuit. In optics, the waveguide plays the same role as the electric conductor (wire) for electronics.

This progress also requires important work regarding the materials and technology to be used. Similar to the development of electronics, the engineering of materials took several decades to develop adequate materials to carry out reliable and effective optoelectronic components. For example, lithium niobate ($LiNbO_3$) is a major dielectric material. It has been used for many years for the fabrication of optoelectronic components for optical signal processing. The use of this material in the form of optical waveguides made it possible in many cases to be released from the limitations related to the use of bulk crystals.

The objective of this book is to provide researchers and students undertaking studies at a Master's level with a teaching aid to understand the basis of integrated optics. This book is a synthesis of theoretical approaches and experimental techniques necessary for the study of the guiding structures. It is based in particular on the research tasks undertaken in this field by the author for about 15 years.

The originality of this book comes from the fact that the ideal models are often accompanied by the experimental tools and their setting to characterize the studied phenomenon. The marriage of the theory and the experiment make the comprehension of the physical phenomena simple and didactic.

The structure of this book is organized into six chapters. Chapter 1 gives the theory of optical waveguides, particularly reporting the study of planar and channel waveguides.

In Chapter 2, the principles of waveguide fabrication techniques are discussed and a review of materials for integrated optics is also reported.

Chapter 3 describes the experimental techniques used for the characterization of guiding structures. The technique of prism coupling – m-line spectroscopy – is described and discussed from theoretical and experimental points of view. The second part of this chapter is devoted to optical losses within the guides, with on the one hand, the presentation of the physical origin of losses and on the other hand, experimental techniques to measure these losses.

The non-linear optical effects in waveguides are covered in Chapter 4. This chapter focuses on second order phenomena and more specifically the second harmonic generation of light.

Chapter 5 is dedicated to the electro-optic effect in waveguides. This chapter covers the electro-optic modulation and its applications in the field of optical telecommunications.

Chapters 4 and 5 present the two theoretical and experimental aspects. The various devices used for the non-linear optical characterization and electro-optics of waveguides are also discussed further.

Finally, Chapter 6 is designed like an introduction to photonic crystals. The photonic crystals are a great part of nano-photonics, which takes an increasingly important place in photonic technologies. This new approach to manipulate the photon will probably provide the ideal solution for allowing integrated optics to make an important technological leap. This chapter is written as an introduction to this field and is far from exhaustive.

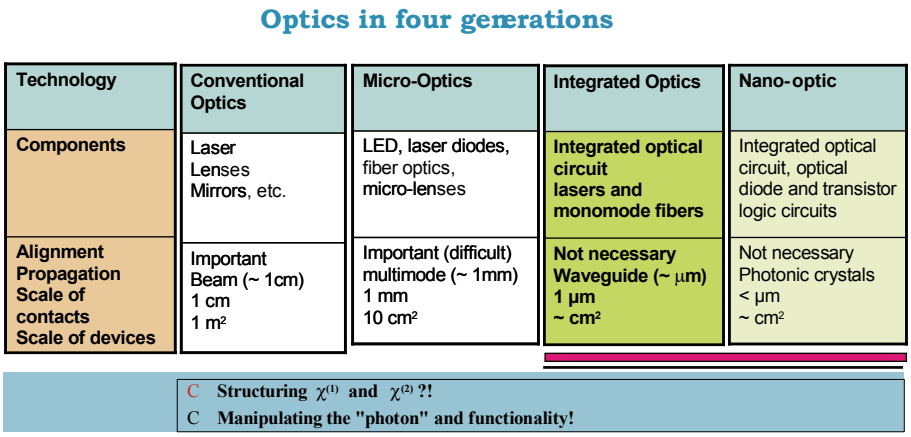

Figure 1. *Summary of the evolution of optics*

3.3. Optical losses

As indicated in the previous sections, the characterization of optical waveguides requires the determination of two essential parameters: the index profile and the thickness of the guiding layer. These two parameters can inform us about the guiding properties of the structure under investigation. Thus, the thickness of the guide directly influences the number of modes, whereas the index profile determines the light confinement performances of the waveguide. However, the development of optical systems requires the development of integrated optical components able to carry on information, from one point to another, with reliability. Therefore, the optical losses within the structure are a vital parameter to completely characterize the waveguide.

In the following section, we will tackle this problem in two essential parts. In the first part we recall the various physical origins of losses in the waveguides. The second part will be devoted to the measurement techniques of this parameter.

3.3.1. *Optical losses origin*

Whatever the fabrication process, optical losses within waveguides can be attributed to four mechanisms [Kad 1989]:

– absorption losses;

– radiation losses;

– conversion losses;

– diffusion losses.

3.3.1.1. *Absorption losses*

Generally speaking absorption losses within dielectric and ferroelectric waveguides, such as $LiNbO_3$ or $LiTaO_3$, can be neglected. However, they might be important in case of semiconductor materials. These absorptions can be related to: interband transitions, free carriers and impurities.

3.3.1.1.1. Interband absorption

In this configuration, photons with energy higher than the material gap can be strongly absorbed, thus producing electronic transitions from the valence band to the conduction band. This phenomenon is more important in semiconductor materials.

3.3.1.1.2. Free carrier absorption

Also called intraband absorption; this occurs when the photons transmit their energy to electrons of the conduction band or to holes of the valence band.

The absorption coefficient, α_{pl}, due to free carriers can be given by the following relation [Che 1987, Kad 1989]:

$$\alpha_{pl} = \frac{k}{n}\Lambda$$

where [3.41]

$$\Lambda = \frac{Ne^3}{m^2 \varepsilon_0 \omega^3 \mu}$$

n: material refractive index
ω, k: pulsation and wavevector, respectively
N: free carriers concentration
e and m: charge and mass of free carriers, respectively
ε_0: the vacuum permittivity
μ: mobility of the free carriers.

3.3.1.1.3. Impurity absorption

In certain cases, during waveguide fabrication, impurities come to contaminate the guiding layer. These impurities could be a source of absorption for certain wavelengths. However, this situation is very rare because waveguide fabrication processes require total control of all the fabrication parameters.

3.3.1.2. *Radiation losses*

In this case, the energy of the guided modes can be dissipated in the substrate or the superstrate. This applies to leaky modes where the value of the effective indices is very close to that of the cut-off index (substrate or superstrate indices). Note however that this only relates to high order modes. It should be noted that by optimizing the fabrication parameters, we can minimize radiation losses which are generally negligible compared with the other losses.

3.3.1.3. *Conversion losses*

In an ideal guiding structure, guided modes are orthogonal and thus energy transfer between modes cannot occur.

However, in certain non-homogenous waveguides, such energy transfers can take place [Mar 1969]. In this case, low order well confined modes can undergo

losses by coupling with other modes of a high order. However, this problem is less frequent in optical waveguides of very good quality and can be omitted.

3.3.1.4. *Diffusion losses*

Diffusion losses are most important and most frequent in waveguides. We can distinguish two types of diffusion losses: volume diffusion losses and surface diffusion losses [Goe 1969, Tie 1971]. The first are caused by the crystalline imperfections and defects in the material. They depend on the concentration of the impurities (diffusion centers) in the crystal. Consequently, these losses are less important than surface diffusion losses, which we will discuss in greater detail. Also, we particularly treat the case of surface diffusion losses.

3.3.1.4.1. Surface diffusion losses

These losses arise from the roughness of the guide-substrate and guide superstrate interfaces. Correction of this problem can be carried out using the optical rays approach: where an optical ray, being propagated in a guiding structure of a thickness d, undergoes multiple reflections on the two interfaces. The number of these reflections over a length L, is given by the following relation [Kad 1989]:

$$N_r = \frac{L}{2d \tan\left(\frac{\pi}{2} - \theta_m\right)} \qquad [3.42]$$

where θ_m is the reflection angle of the guided mode m.

Diffusion losses appear for each reflection and are important for high order modes because the number of reflection increases according to the order of the modes (θ_m decreases).

For a qualitative description of these losses, we use the attenuation coefficient α_d, which shows that the intensity of the guided mode at a distance z can be put into the following form:

$$I(z) = I_0 \exp(-\alpha z) \qquad [3.43]$$

where I_0 is the initial intensity at $z = 0$.

Coefficient α can be calculated using several methods [Kad 1989, Che 1987, Mar 1969, Goe 1969, Tie 1971]. The simplest one, developed by P.K. Tien [Tie 1971], is based on the Rayleigh's criterion, according to which for an incident

optical power Pi on a surface, the reflected power in a specular direction can be given by the following relation:

$$P_r = P_i \exp\left[-\left(\frac{4\pi\sigma\cos\theta_m}{\lambda}\right)^2\right] \qquad [3.44]$$

where σ is the standard deviation of the amplitudes of thickness fluctuations.

Under these conditions, P. K. Tien showed that the attenuation coefficient could be written:

$$\alpha = A^2\left(\frac{\cos^3\theta_m}{2\sin\theta_m}\right)\left(\frac{1}{d_{eff}}\right) \text{ cm}^{-1} \qquad [3.45]$$

$$\text{where } A = \frac{4\pi}{\lambda}\sqrt{\sigma^2_{(n,n_a)} + \sigma^2_{(n,n_s)}} \qquad [3.46]$$

and d_{eff} is the effective thickness.

Note that coefficient α_d, given by formula [3.45], is proportional to the square of the ratio of material roughness to the wavelength. We can also show that optical losses in dB.cm^{-1} can be calculated using the following relation:

$$a = 4.3\alpha \quad (\text{dB.cm}^{-1}) \qquad [3.47]$$

As a whole, surface diffusion optical losses are generally dominant in dielectric waveguides, such as glasses and oxides. They are of 0.5 to 5 dB.cm^{-1} for low order modes, which increases for high order modes [Tie 1971]. In semiconductors, these losses are less important due to the very minor roughness of the guiding layer (less than 0.01 μm).

3.3.2. *Optical loss measurements*

The basic principle of these measurements consists of comparing the power of the light which is propagated in the guide with the power of the light at launching. However, in practice, many problems emerge, in particular those due to the coupling

and the decoupling, which introduce extra losses that are generally difficult to manage. In addition, a rigorous study of the problem requires the knowledge of the origin of losses which makes it more complicated.

The developed measurement techniques depend, particularly, on the coupling method used according to the guide considered, the nature of the losses, and their importance in the measured losses.

In this section, we will point out the principles of these techniques which generally consist of measuring the attenuation coefficient according to the waveguide length.

3.3.2.1. *End-fire coupling technique*

This simple technique uses end-coupling, as indicated in Figure 3.18. The principle compares the transmittance of several samples of different lengths in order to determine the attenuation coefficient α.

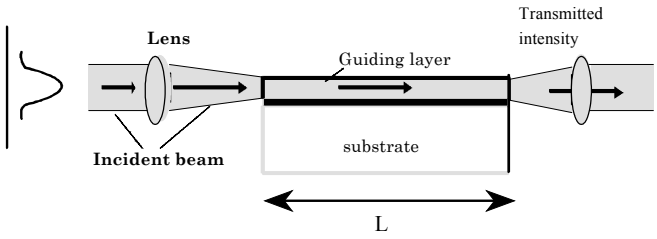

Figure 3.18. *Loss measurements by the end-coupling method*

In practice, it is very difficult to obtain a series of waveguides of the same optical quality and thus the comparison is not compatible. Consequently, it is necessary to cut the same guide for each measurement. Generally, we start with a rather important length L_0. The light is injected into the guide using an objective microscope, or even an optical fiber, as indicated in Figure 3.18. The attenuation coefficient can be written in the following way:

$$\alpha = \frac{\ln\left(\frac{p_0}{p_1}\right)}{L_0 - L_1} \qquad [3.48]$$

where L_0, L_1 and P_0, P_1 are lengths and transmitted powers, respectively, before and after the sample cut.

As an example, F. P. Strohkendl *et al.* [Str 1991] reported optical losses of 3 $dB.cm^{-1}$ in $KNbO_3$ He^+-implanted waveguides using this technique. D. Kip *et al.* [Kip 1995] also reported the optical losses investigation of SBN proton-implanted waveguides using the same principle [Brü 1995]

Nevertheless, the utilization of this technique is somehow limited due to many disadvantages. These arise from the coupling method employed as previously mentioned, and can be summarized as follows:

– it is a destructive method (the guide should be cut for each measurement);

– it is a non-selective method (all the guided modes are simultaneously excited);

– it is difficult to carry out because it needs precise alignment of the experimental set-up, as well as high optical polishing of the guide sections.

3.3.2.2. *Prism coupling method*

This method has been extensively applied to different configurations and is a good alternative to the end-fire coupling technique. As indicated in Figure 3.19, a first prism is used to inject light into the guide, while the second is used to out-couple this light, allowing for the transmitted intensity (guided) measurement. Generally speaking, the first prism is fixed, whereas the second is moved along the guide. Several measurements at different waveguide lengths make it possible to determine the attenuation coefficient according to length L.

The displacement, however, of the out-coupling prism may introduce additional experimental errors. To avoid this situation, we use a third prism [Aru 1986, Web 1973, Won 1980], as shown in Figure 3.19.

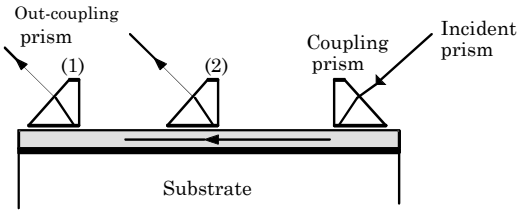

Figure 3.19. *Prism coupling method of optical loss measurement*

Y.H. Won *et al.* [Won 1980] showed that the out-coupled intensity from the third prism is independent of the coupling coefficients and can be written as:

$$I(z) = \frac{P_2 P_3^0}{\Delta P} \qquad [3.49]$$

with:

$$\Delta P = P_3^0 - P_2 \qquad [3.50]$$

$P_2{}^0$: light power out-coupled from the second prism without the third prism

P_3: light power out-coupled from the third prism.

This method allows selective measurements, in the sense that we can selectively excite the waveguide guided modes. It is also a non-destructive method (the sample does not need to be cut). However, it is difficult to exactly reproduce the same coupling and out-coupling conditions for the three prisms. Thus, the accuracy of the measurements can be affected.

It is worth noting that a matching liquid of low index (n = 1.33, glycerin n = 1.47) can be used to improve the method performances.

3.3.2.3. *Prism coupling and end-fire out-coupling method*

In this configuration, the prism coupling is used to launch light into the waveguide, and the end-fire out-coupling is used to measure the transmitted light (see Figure 3.20). The latter is performed versus the guide length by moving the coupling prism upon the surface of the waveguide [Bou 1997]. At the same time, the reflected intensity on the prism base is measured in order to determine the coupling coefficient. Under these conditions, we can escape from the coupling coefficient influence.

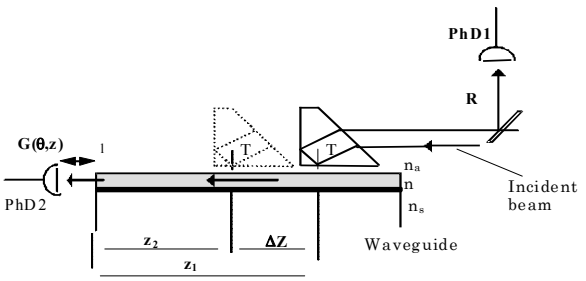

Figure 3.20. *Loss measurement by prism-coupling and end-fire out-coupling*

Two photo-detectors (PhD1) and (PhD2) are used to simultaneously measure the reflected and transmitted intensities. For instance, for waveguide length z, we can write:

$$P_m(z) = \eta_m T_m \exp(-\alpha_m z) \quad [3.51]$$

where η_m is the coupling coefficient; α_m is the attenuation coefficient for the m^{th} mode; $P_m(z)$ is the guided intensity of the m^{th} mode; and T_m is the injected intensity into the prism.

Thus, we can write for z_1 and z_2:

$$P_m(z_1) = \eta_m T_m \exp(-\alpha_m z_1) \quad [3.52]$$

$$P_m(z_2) = \eta'_m T_m \exp(-\alpha_m z_2) \quad [3.53]$$

Generally, η(m) and η'(m) are different because the coupling conditions are different. However, this method makes it possible to be completely released from this parameter using the two measurement systems (reflection (PhD1) and transmission (PhD2)) simultaneously [Bou 1997].

We start by measuring the transmitted and the reflected intensities for length z_1. Then, before taking a second measurement of the transmitted intensity for length z_2, we adjust the coupling conditions, in particular the air-gap in order to maintain the same initial coupling conditions as for position z_1. For this, we measure the guided modes spectrum by reflection, which can be compared with the spectrum obtained for position z_1. As an example, Figure 3.21 shows the TM guided modes spectra obtained by reflection in a $LiNbO_3$ He+-implanted waveguide.

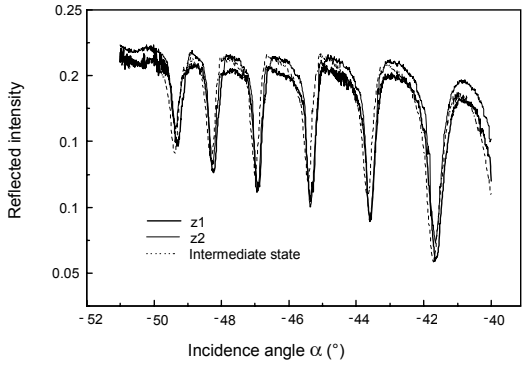

Figure 3.21. *Prism coupling conditions controlled using the reflected intensity measurements*

The superposition of the two guided modes spectra allows us to call the coupling coefficients identical at positions z_1 and z_2. Therefore, η (m) = η'(m). In addition to this, it is important to maintain as constant the distance between the photo-detector (PhD2) and the waveguide end, Figure 3.20, as well as to highly polish the waveguide sections. Under these conditions, light diffusion at the sample extremities can be disregarded. Finally, from relations [3.51] and [3.52], the attenuation coefficient is given by:

$$\alpha_m = \frac{1}{(z_1 - z_2)} \ln\left[\frac{P_m(z_2)}{P_m(z_1)}\right] \quad (\text{cm}^{-1}) \qquad [3.54]$$

This relation is independent of the coupling coefficient. It also allows us to obtain the absolute error $\Delta\alpha$:

$$\Delta\alpha = \frac{2\Delta z}{(z_1 - z_2)^2} \ln\left[\frac{P_m(z_2)}{P_m(z_1)}\right] (\text{cm}^{-1}) \qquad [3.55]$$

where Δz is the absolute error of the guide length z measurements.

This technique was used to measure optical losses in $LiNbO_3$ (He^+, H^+)-implanted waveguides [Bou 1997] and $Li_2B_4O_7$ He^+-implanted waveguides [Bou 2001]. Results indicated optical losses of the order of dB.cm^{-1}.

From relation [3.55], it appears that the measurement accuracy depends in particular on the absolute error of the waveguide length measurement. Therefore, longer samples produce high accuracy results. As a matter of fact, this technique allows us to measure optical losses of 0.1 dB.cm^{-1}.

3.3.2.4 *Surface analysis method*

The techniques previously discussed determine the total losses in the guide, without distinction between the origins of these losses: absorption, radiation, diffusion or conversion. For dielectric waveguides, where the losses by diffusion are dominant, the analysis of the surface of the guide makes it possible to determine the attenuation coefficient. For a uniform guide, the scattered light from the surface can be considered proportional to the guided intensity.

Measurement of the scattered light can be carried out using an optical fiber, (Figure 3.22). A surface waveguide analysis gives the diffused intensity according to the guide length [Oka 1983, Oka 1985, Roe 2004, Ros 1995]. The slope of the obtained curve determines the attenuation coefficient.

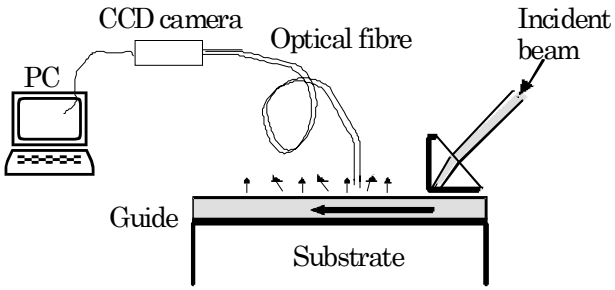

Figure 3.22. *Surface analysis method for determining optical losses*

Note that, we can also use a CCD camera in order to directly collect the scattered light from the waveguide surface [Ros 1995].

For instance, Figure 3.23 displays a photograph of the propagated light into a planar (a) and a channel (b) optical waveguide of $Ca_4YO(BO_3)_3$ (YCOB) He^+-implanted waveguide [Vin 2004].

Figure 3.23. *Photograph of light propagation of (a) planar and (b) channel YCOB He+-implanted waveguide([Vin 2004])*

The analysis of the intensity variation according to the propagation distance (Figure 3.24) makes it possible to obtain diffusion optical losses. For instance, Vincent *et al.* reported losses of 2 $dB.cm^{-1}$ and 1.8 $dB.cm^{-1}$ in planar and channel waveguides, respectively.

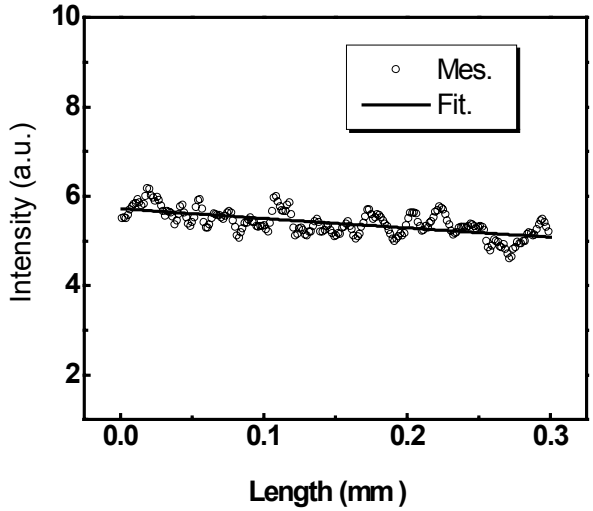

Figure 3.24. *Evolution of the intensity of the guided light according to the propagation length: guide plan YCOB:He+ ([Vin 2004])*

This technique is a non-destructive method as no contact is needed in order to perform measurements. However, its utilization is limited to waveguides where the losses by diffusion are more important than losses by absorption or radiation.

3.3.3. *Characterization in near-field microscopy of optical waveguides*

Scanning near-field optical microscopy (SNOM) makes it possible to observe small details of physical objects, as well as to determine of the electromagnetic field distribution on the sample surfaces, with a sub-wavelength resolution. This technique has been used extensively recently in different configurations. Its application to the study of sub-micron dimensions is of great interest from the fundamental point of view as well as for the characterization and the study of optical compounds. The use of this technique (SNOM) for the study of light confinement in various optoelectronics structures has already been the subject of several publications [Bor 2000, Bou 1992, For 1998, Tas 2002].

The SNOM configuration used is that of near-field collection mode, with a tapered and metallized optical fiber. The evanescent field collected on the surface of the guide is sent towards a photo-detector. The experimental setup is displayed in Figure 3.25.

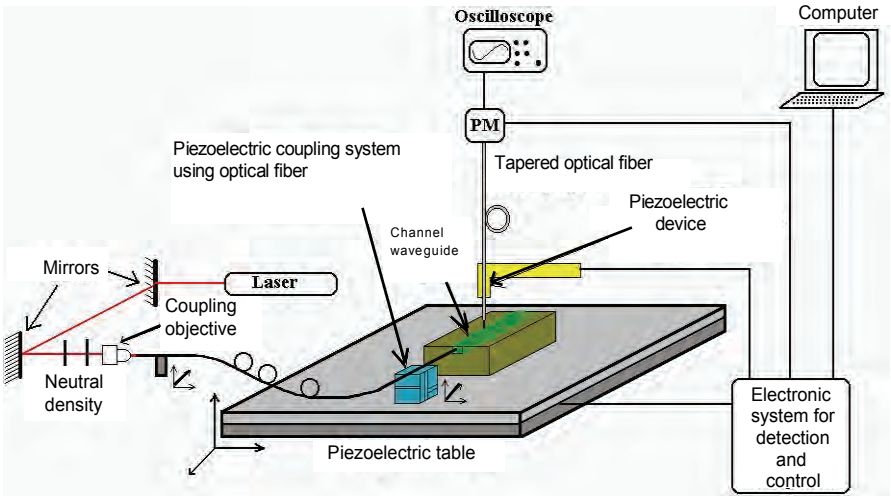

Figure 3.25. *SNOM setup for optical waveguide characterization*

Figure 3.26 reports the topographic and optical images of the exchanged $LiTaO_3$ waveguide. Several images were taken and assembled in order to obtain a total image of the guide over a length of a millimeter. We can note that this study shows that the protonic exchange process produces a dilatation of the crystal in the exchanged zone. Moreover, we observe a light topography of approximately 5 nm on each side of the exchanged zone.

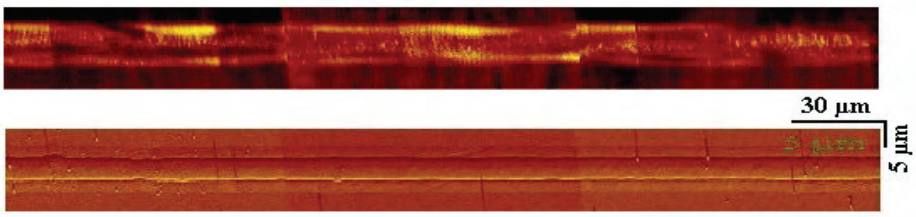

Figure 3.26. *SNOM optical image (top) and topographic image (bottom) of a channel guide of* $LiTaO_3$

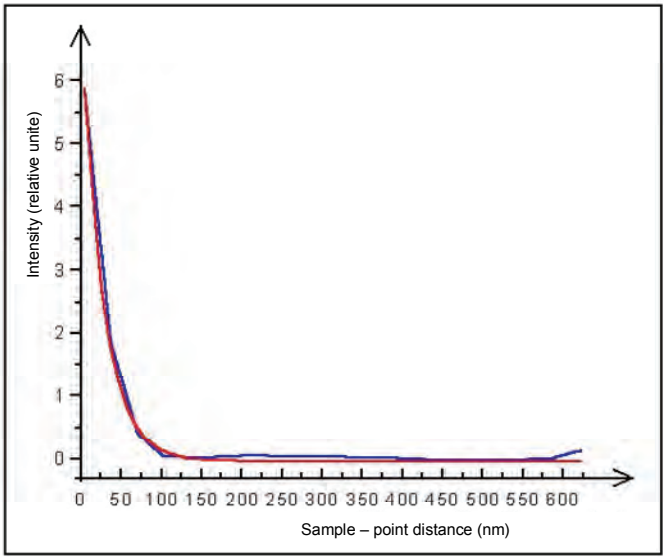

Figure 3.27. *Variation of the evanescent field according to the length of the sample*

Figure 3.27 shows the exponential decay of the evanescent field intensity along the waveguide surface. From this curve, it is possible to deduce the effective index n_{eff} of the guide using the following relation (λ is the working wavelength and I the evanescent field intensity) [Bor 2000, Cam 2002].

$$I(z) = I_0 \exp\left(-4\pi z\sqrt{n_{eff}^2 - 1}/\lambda\right) \qquad [3.56]$$

The curve analysis gives n_{eff} of 2.14. This value is in close agreement with the theoretical value of the extraordinary index of $LiTaO_3$ at $\lambda = 632.8$ nm ($n_{eo} = 2.19$).

3.4. Bibliography

[Aru 1986] Arutunyan E.A. and. Galoyan S.K, "New method for loss measurements in optical waveguides", *Optic. Com*., 57(6), 391-393 (1986).

[Bor 2000] Borrisé X., Jiménez D., Barniol N., Pérez-Murano F., Aymerich X., "Scanning near field optical microscope for the characterization of optical integrated waveguides", *Journal of Lightwave Technology*, 18(3), 370-374 (2000).

5.6. Integrated optic setups using the electro-optic effect

In optical communication networks, external modulators, in particular those using the electro-optic effect, play a very important role. EO modulators exist in several forms and use different materials. However, EO modulators based on $LiNbO_3$ are particularly interesting because of the performances they offer. Integrated components usually work with low command voltage and offer very high modulation frequencies. Waveguides are obtained by Ti diffusion or by ionic exchange. The coupling is often performed using an optical fiber [Woo 1993, Naz 1993, Bin 2006, Bin 2003, Cou 2002].

The benefits of integrated devices based on waveguides compared with those based on bulk components comes from the fact that limitations linked to the diffraction of the laser beam can be totally eliminated thanks to the light confinement in the guide. Consequently, the propagation of guided waves can be easily controlled and numerous guide configurations can be used offering diverse and varied functions.

Within the framework of this book, we will limit ourselves to the presentation of two examples of integrated EO modulators, namely phase and intensity modulators. Interested readers will find more examples in numerous publications dealing with the subject [Tam 1990].

However, EO components based on waveguides are fabricated, in particular, by using specific and appropriate electrode configurations. To do this, a preliminary study of the distribution of the electric field according to the geometry of the electrodes is often necessary.

5.6.1. *Optimal design of the electrodes for integrated EO modulators*

The electric field in the waveguide is obtained using two co-planar electrodes as shown in Figure 5.17. In this case, the knowledge of the distribution of the electric field and its recovery with the electric field of the optical wave is essential for improved functioning of the modulator. The optimization of the design of the electrodes was, amongst others, reported by Marcuse et al. [Mar 1982]. In integrated optics, modulators use one or two waveguides generally channels and preferably monomodes. The application of an electric field modifies the propagation constant of the guided mode through the variation of the refraction index by the EO effect.

In this section, a few basic notions will be given about the design of electrodes for integrated EO modulators. A detailed analysis of the different possible configurations requires a specific study which goes beyond the framework of this

book. For further details, the reader can refer to numerous references which deal with this subject [Bin 2003, Cou 2002].

For $LiNbO_3$, the variation undergone by the index and also by the propagation constant depends on the direction of the applied electric field compared with the direction of the optical axis. As shown in previous paragraphs, the optimum situation consists of applying an electric field parallel to the optical axis of the crystal. However, two questions are still to be solved. The first deals with the optimum geometry of the electrodes in terms of interelectrodes space and dimensions (widths and thickness). The second question deals with the optimum position of the guide beneath the electrodes to obtain the maximum EO effect [Bin 2003, Bin 2006, Cou 2002, Hui 1998, Lee 2003, Liu 1982, Ran 1992]. This question is important, particularly when the phases of the two TE and TM polarizations must be adjusted by the applied field.

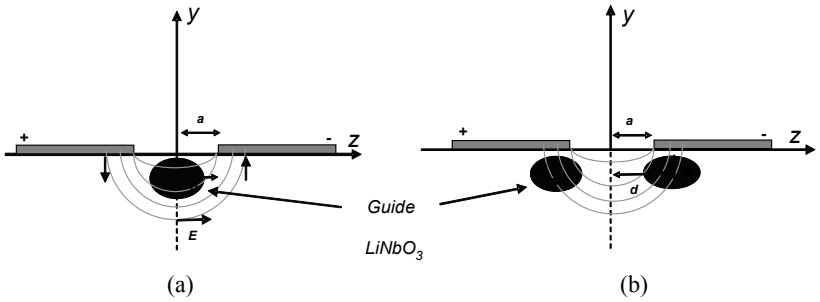

Figure 5.27. *Geometry of the semi-infinite electrodes above: (a) one guide; and (b) two waveguides*

In the case of two semi-infinite electrodes in Figure 5.27a, the position of the channel guide depends on the cut of the crystal and on the interelectrodes space, as well as on the component of the electric field to be used. This issue was the focus of section 5.2.1. The distribution of the electric field is given by relations [5.59] and illustrated by Figure 5.7.

For a z-cut crystal with the optical axis perpendicular to the surface, the optimum position of the guide is near the tip of one of the two electrodes ($d > a$), where the vertical component of the field is maximum. However, if it is a y-cut crystal (the optical axis being parallel to the surface), the waveguide must be placed in the middle of the interelectrode space where the horizontal component E_z of the electric field is maximum (see Figure 5.27a). Nevertheless, in this case, if the interelectrodes space is very big compared to the dimensions of the guide, the

optimum position of the guide is slightly closer to one of the two electrodes with $d<a$.

Figure 5.27b illustrates the possibility of using two guides, each set beneath one of the two electrodes (see Figure 5.27b). Here, the two EO effects are reversed because of the direction of the electric field. This creates a directional coupler via the "push-pull" effect. In this situation, it is important to have a minimum interelectrode space. However, it is not necessary to place the tips of the two electrodes strictly above the center of the two guides.

In practice, the semi-infinite electrodes are not really used and the situation described so far represent an approximation of the issue. The electrodes usually have widths comparable to the interelectrodes space (see Figure 5.28).

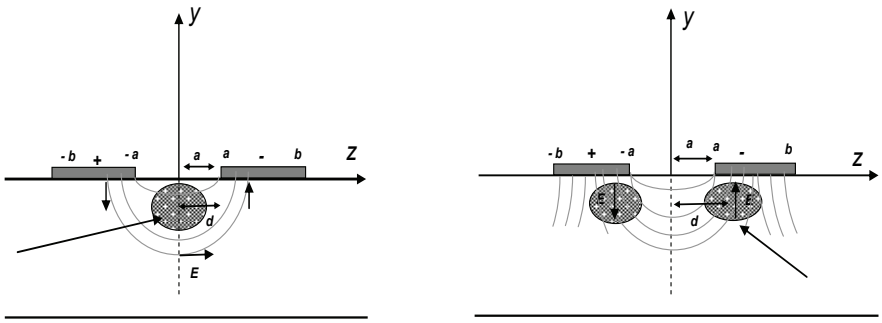

Figure 5.28. *Geometry of finite dimension electrodes: (a) one guide and (b) two waveguides*

For two finite electrodes, we can show that the two components of the electric field are given by [Mar 1982, Ram 1982, Van 1974, Liu 1982]:

$$E_z = -\frac{U}{2aK}\frac{\cos(\Phi)}{\left(A^2 + B^2\right)^{\frac{1}{4}}}$$
$$E_y = \frac{U}{2aK}\sqrt{\frac{\varepsilon_z}{\varepsilon_y}}\frac{\sin(\Phi)}{\left(A^2 + B^2\right)^{\frac{1}{4}}} \qquad [5.128]$$

with:

$$A = \left(1 - \frac{k^2}{a^2}(z^2 - y^2)\right)\left(1 - \frac{1}{a^2}(z^2 - y^2)\right) - 4\frac{k^2}{a^4}z^2y^2$$
$$B = -2\frac{k^2}{a^2}zy\left(1 - \frac{1}{a^2}(z^2 - y^2)\right) - 2\frac{1}{a^2}zy\left(1 - \frac{k^2}{a^2}(z^2 - y^2)\right) \qquad [5.129]$$
$$\Phi = -\frac{1}{2}\arctan\left(\frac{B}{A}\right)$$

Figure 5.29 shows the evolution of the electric field vector obtained in this electrodes configuration. Use of the previous equations enables us to calculate the variation of the index in the guide according to its position in comparison with the two electrodes.

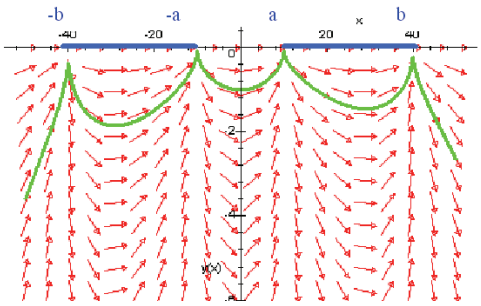

Figure 5.29. *Distribution of the electric field obtained by two finite dimension electrodes*

Note that component E_z varies very little according to depth, and almost does not vary according to z if it in the middle of the electrodes. Moreover, component E_y has a negligible variation according to y or z, if it is in the middle of the electrodes.

It is interesting to note that in most cases, it is necessary to place silica as a buffer layer between the optical guides and the electrodes, in order to minimize the influence of the metallic layer on the optical wave propagation. The drawback of using this layer is related to the command voltage, which must be increased because the electric field seen by the guide is weakened [Chu 1993, Sab 1986].

5.6.2. *Integrated EO phase modulator*

We saw in section 5.5 that in a bulk EO modulator, phase mismatching induced by EO effect is given by:

$$\Delta\varphi = \pi \frac{V}{V_\pi} = \frac{\pi L}{\lambda_0} r_{eff} n_{eff}^3 \frac{V}{d} \qquad [5.130]$$

In the case of an EO modulator based on waveguides, this relation is no longer valid as it is. In fact, on one hand the two coplanar electrodes induce an inhomogenous electric field in the guide which is far different from *V*/*d* (see previous section); and on the other hand the guided propagation imposes the existence of proper modes with propagation constants and a distribution of the optical field according to the guided mode. Under these conditions we must think in terms of the effective index of guided modes and of recovery between the electric field and the optical field [Kim 1989].

In an EO modulator based on a waveguide, phase mismatch becomes:

$$\Delta\varphi = \Delta\beta_m L = \frac{2\pi}{\lambda_0} \Delta N_m L \qquad [5.131]$$

where $\Delta\beta_m$ and ΔN_m are the variations induced by the EO effect of the propagation constant and the effective index of the mode m, respectively.

From the dispersion equation of guided modes (explained in Chapter 1), it is possible to write:

$$\Delta N_m = \Gamma\ \Delta n \qquad [5.132]$$

Γ being the factor of proportionality between the index variation by EO effect and the modification of the effective index of the resulting mode. This factor is always < 1 and it is weaker when the mode is near the cut-off [Tam 1990].

In the same way, the variation of the refractive index induced by two coplanar electrodes is written:

$$\Delta n = \frac{1}{2} r_{eff} n_{eff}^3 \frac{V}{a} \Gamma_{ovl} \qquad [5.133]$$

where Γ_{ovl} is a factor of reduction due to the recovery between the electric and optical fields. This is given by the overlap integral:

$$\Gamma_{ovl} = \frac{\iint E_{op}^2(y,z) E_{el}(y,z) dydz}{\iint E_{op}^2(y,z) dydz} \qquad [5.134]$$

This factor is also less than 1, its value depending notably on the width separating the two electrodes.

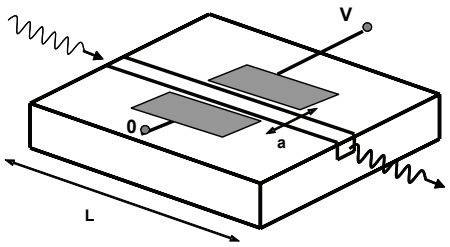

Figure 5.30. *Phase modulator in integrated optics*

If we consider a the interelectrode space and l their length, as a first approximation the half-wave voltage can be written:

$$V_\pi = \frac{\lambda_0}{\Gamma\, \Gamma_{ovl} r_{eff} n_{eff}^3} \frac{a}{l} \qquad [5.135]$$

With the utmost rigor, the analysis of the distribution of the electric field, which was developed in section 5.2.1 should be used. Nevertheless it is possible to realize from equation [5.135] that the ratio $\frac{a}{l}$ is very low, thus the half-wave voltage is within the order of a few volts. The functioning of this type of modulator has been shown for frequencies higher than 100 GHz.

Interestingly, the waveguide must be essentially monomode. The existence of several guided modes reduces the performances of the modulator and complicates its design. The EO coefficient r_{eff} which intervenes depends on the relative positions of the electrodes, on their widths and of the position on the guide (of the guided mode) in comparison with them.

5.6.3. *Integrated EO intensity modulator (Mach-Zehnder)*

This component was described in section 5.3.1, as well as in the presentation of bulk EO intensity modulators (see section 5.4.2). The basic principle consists of using two Y-junctions face to face as shown in the following figures. The two electrodes are placed either on one of the arms of the Mach-Zehnder (see Figure 5.31a) or above both arms (see Figure 5.31b). The position of the two guides in comparison with the electrodes must be carefully analyzed and made according to the performances and the application desired. See, for instance, section 5.5.1.

Let us consider a z-cut $LiNbO_3$ crystal. By applying a voltage to the electrodes in Figure 5.31b and in the case of the TM_{00} guided mode, the mode propagating in the upper arm undergoes a phase mismatch of $+\Delta\varphi$ and interferes with the mode propagating in the lower arm, which undergoes a phase mismatch of $-\Delta\varphi$. The total phase mismatch between the two modes in both arms is $2\Delta\varphi$.

Finally, the phase mismatch is written:

$$\begin{aligned} 2\Delta\varphi &= \pi \frac{V}{V_\pi} \\ V_\pi &= \frac{\lambda_0}{2\Gamma\, \Gamma_{ovl} r_{33} n_e^3} \frac{a}{l} \end{aligned} \qquad [5.136]$$

Through a simple analysis based on the interference phenomenon between two electromagnetic waves, we can show that intensity at the output of the modulator is [Tam 1990]:

$$P_s = \frac{P_e}{2}\left[\frac{\left(1-\sqrt{r}\right)^2}{1+r} + 4\frac{\sqrt{r}}{1+r}\cos^2\left(\frac{\pi}{2}\frac{V}{V_\pi}\right)\right] \qquad [5.137]$$

where r is the ratio of the intensities between the two arms of the Mach-Zehnder ($r = I_1/I_2$). From the previous equation, the extinction ratio is given by:

$$E = 10\log\frac{P_s(\max)}{P_s(\min)} = 10\log\left(\frac{1+\sqrt{r}}{1-\sqrt{r}}\right)^2 \quad (dB) \qquad [5.138]$$

Note that the extinction ratio of the modulator depends particularly on the intensity ratio between the two arms. If the ratio tends towards 1, the extinction ratio tends towards the infinity. For example, if $r = 2$, the extinction ratio $E = 15$ dB. In this particular case (z-cut $LiNbO_3$), the half-wave voltage can be very low, in the order of a few volts according to the dimensions and the space between the electrodes.

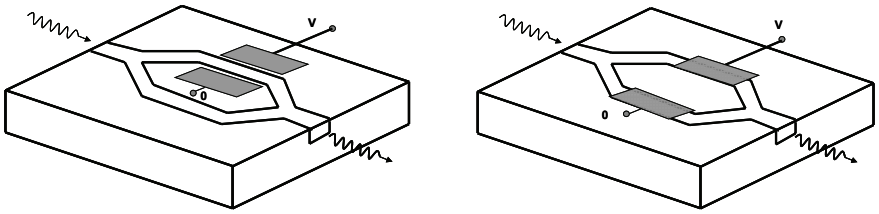

(a) (b)

Figure 5.31. *Diagram of the principle of a Mach-Zehnder modulator in integrated EO*

Let us also note that the fabrication of this type of modulator is currently very well developed and that Y-junctions can be obtained precisely. In practice losses in this type of junction can be minimized by adjusting the junction angle. In the same way by choosing a suitable electrode configuration (i.e. by placing two sets of electrodes on both arms), we can make the modulator independent of light polarization.

Finally, high bandwidth can be obtained using this type of EO modulator in the configuration described in section 5.4.2.2.1, that is to say, with a traveling electric wave as shown in Figures 5.32a and b. In this case the bandwidth is determined by the phase matching between the optical wave and the radio frequency wave.

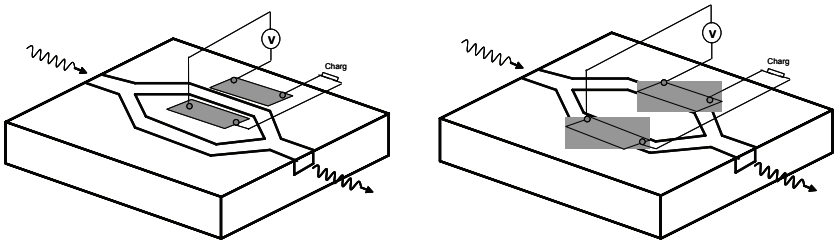

(a) (b)

Figure 5.32. *Diagram of the principle of a Mach-Zehnder modulator with an integrated traveling wave*

Our presentation of integrated EO modulators is far from exhaustive and remains obviously simplified. In fact, a detailed analysis requires us to take into account other factors linked notably to the functioning of the EO modulator, such as drift and chirp issues. Modulators need to be maintained in the linear region of their EO characteristics. However, the functioning point can undergo a shift or drift in time due to a slow variation of the phase between the arms of the Mach-Zehnder.

A rigorous study of EO modulators also demands an electrical component approach. In fact, the performances of the EO modulator strongly depend on the structure of the electrodes used. The most frequently used structure is the one based on traveling wave electrodes. For example, if a push-pull configuration is considered, the potential difference is applied between the central electrode and the mass electrodes (see Figure 5.33a). In this case, the electrodes can be represented by a transmission line (see Figure 5.33b) [Cou 2002].

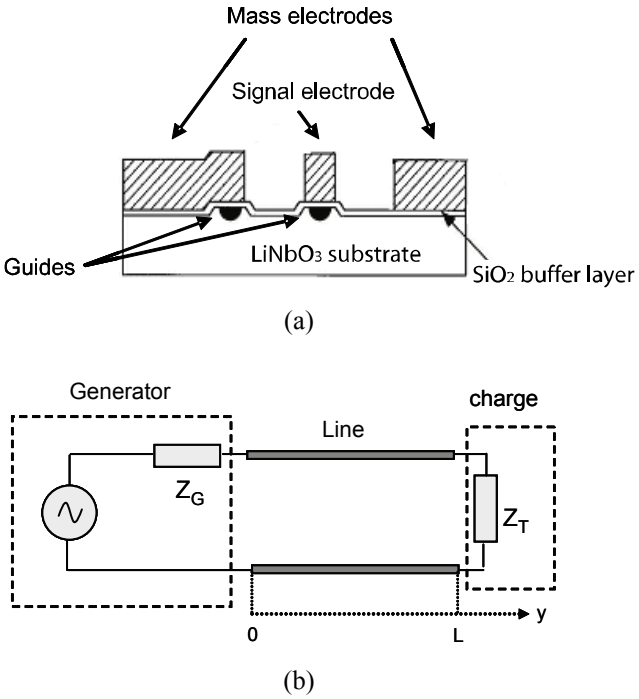

Figure 5.33. *The principle of a Mach-Zehnder modulator and its equivalent diagram in the form of a transmission line*

A transmission line is a structure with two conductors supplied by a voltage generator of intern impedance Z_G, completed by a Z_T (see Figure 5.33b). A simplified study of the transmission line supposes that it is ideal:

– the conductors have an infinite conductivity, in other words the electric and magnetic fields do not penetrate the conductor;

– the line is considered infinite, so length L is greater than the waveguide;

– the line is surrounded by a homogenous and isotropic dielectric.

Under these conditions, the electric and magnetic fields are transversal and the propagation equations of the electromagnetic field are then equivalent to the propagation of the current i and the potential u, in a line composed of elementary and tiny sections (length dy), as illustrated in Figure 5.34.

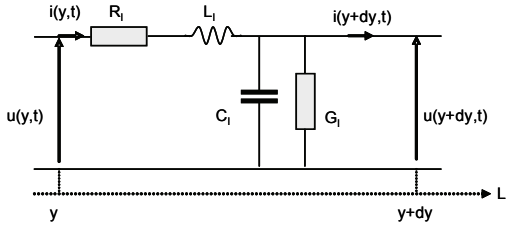

Figure 5.34. *Equivalent electric diagram*

Each elementary section is characterized by the following parameters:

– lineic resistance R_l (Ω/m), which represents losses by conduction;

– lineic inductance L_l (H/m) due to the magnetic field inter and intra conductors;

– lineic capacity C_l (F/m) formed by the dielectric and the two conductors, represents active energy losses in the dielectric;

– lineic conductance G_l (S/m) due to the insulating defects and to the dielectric losses, represents reactive energy losses in the dielectric.

A simplified study of this problem enables us to determine the characteristic parameters of the transmission line and consequently of the EO modulator. We will describe the outline of this investigation.

In a sinusoidal system, we can define a complex voltage and current:

$$\begin{aligned} \underline{u}(y,t) &= \underline{U}(y)\exp(j\omega t) \\ \underline{i}(y,t) &= I(y)\exp(j\omega t) \end{aligned} \qquad [5.139]$$

The equations of the lines are:

$$\begin{aligned} &\frac{d^2\underline{U}(y)}{dy^2} - Z_l Y_l \, \underline{U}(y) = 0 \\ &\frac{d^2\underline{I}(y)}{dy^2} - Z_l Y_l \, \underline{I}(y) = 0 \end{aligned} \qquad [5.140]$$

with $Z_l = R_l + L_l\omega$ and $Y_l = G_l + jC_l\omega$.

The general solution:

$$\begin{aligned} \underline{U}(y) &= \underline{U_I}\exp(-\gamma y) + \underline{U_R}\exp(-\gamma y) \\ \underline{I}(y) &= \underline{I_I}\exp(-\gamma y) + \underline{I_R}\exp(-\gamma y) \end{aligned} \qquad [5.141]$$

where U_I and $\underline{I_I}$ are the amplitudes of the incident wave and $\underline{U_R}$ and $\underline{I_R}$ are the amplitudes of the reflected wave.

We define the complex propagation constant by:

$$\gamma = \sqrt{Z_l Y_l} = \alpha + j\beta \qquad [5.142]$$

with α the attenuation (lineic attenuation coefficient) and β the lineic phase mismatch.

If the line is without losses: $R_l = 0$ and $G_l = 0$, consequently $\alpha = 0$, and we obtain:

$$\beta = \omega\sqrt{C_l L_l} \qquad [5.143]$$

The secondary parameters of the line are characteristic impedance Z_c, the electric effective index n_{eff} and the attenuation coefficient α. These parameters characterize, respectively, the reflection at the end of the line, the propagation velocity of the signal and the diminution of the amplitude propagating. The characteristic impedance $Z_c(\Omega)$ is defined by the following expression:

$$Z_c = \sqrt{\frac{Z_l}{Y_l}} = \sqrt{\frac{R_l + j\omega L_l}{G_l + j\omega C_l}} \qquad [5.144]$$

If the line is without losses, the impedance is purely real:

$$Z_c = \sqrt{\frac{L_l}{C_l}} \qquad [5.145]$$

The effective electric index is given by:

$$n_{eff} = \frac{v_\varphi}{c} = \frac{1}{c\sqrt{C_l\, L_l}} \qquad [5.146]$$

The attenuation coefficient α, which characterizes losses in transmission lines, is related to several phenomena:

– *Conduction losses* (resistive losses or metallic losses) are given by relation:

$$\alpha_c = \frac{R_l\,(f)}{2Z_c} \qquad [5.147]$$

R: resistance of the conductor

Z_C: characteristic impedance

Conduction losses are linked to the skin-effect. Namely, for a high frequency, current is located in a thickness (δ) called skin thickness. A current density appears on a thickness of the metal (δ) given by:

$$\delta = \sqrt{\frac{\rho}{\pi\mu f}} \qquad [5.148]$$

ρ: resistivity of the current or the conductor (Ω.m)

$\mu = \mu_r\, \mu_o$: magnetic permeability of the conductor

$\mu_o = 4\text{x}\pi\text{x}10^{-7}$ H/m: permeability of the vacuum

μ_r: relative permeability

f: frequency (Hz).

Note that conduction losses (α_c) increase proportionally to the square root of the frequency, and represent the main cause of attenuation of the electric wave.

– *Dielectric losses* (dielectric attenuation) are due to the charge leakage in the dielectric when it is not completely insulated:

$$\alpha_d = \frac{\omega}{2}\sqrt{\mu_{\grave{a}}\mu_r}\ \tan\delta_d \qquad [5.149]$$

where *tan* δ_d is the ratio between *Im*(ε) and *Re*(ε) which depends on the frequency.

It is interesting to note that dielectric losses cannot be neglected at high frequencies.

As a whole, characteristic parameters of the transmission line (of the electrodes), which are attenuation α, impedance Z_c, and effective index n_{eff}, are determined from in line primary parameters (R_l, L_l, C_l and G_l), which in turn are defined by the structure of the electrodes. These parameters directly influence the functioning of the EO modulator and more specifically the bandwidth and the chirp.

In fact, the amplitude modulation of an optical signal can be accompanied by a parasite frequency modulation called "*chirp*". The modification of the spectrum obtained can modify the signal envelop propagating in the fiber.

The chirp depends in particular on the characteristics of the arms of the Mach-Zehnder, and on the cut of the $LiNbO_3$ used in order to have the same EO interaction on each arm of the Mach-Zehnder [Kaw 2001, Kim 2002, Shi 1994]. Another parameter that can also influence the chirp of a modulator is the extinction ratio, which depends, among other things, on the losses in the two arms of the modulator. The control of these different factors requires much attention both at the level of the waveguide fabrication process and at the level of the management of applied voltages as well as the electronic circuits used.

The chirp parameter, which indicates a variation of the carrying frequency of the optical signal is generally defined from the phase and intensity of the optical wave as follows:

$$\alpha = \frac{\dfrac{d\Phi}{dt}}{\dfrac{1}{E}\dfrac{dE}{dt}} \qquad [5.150]$$

where E is the amplitude of the electric field of the optical wave and Φ is the phase mismatch induced by the modulator.

From this expression we infer:

$$\alpha = -\cos(\Delta\Phi)\left(\frac{A_1 + A_2}{A_1 - A_2}\right) \qquad [5.151]$$

where A_1, A_2 are amplitudes of the optical phase induced by the applied electric field in each arm of the structure Mach-Zehnder structure.

In the case of small amplitude of modulation (A_1, A_2 <<1) and if $\Phi = -\frac{\pi}{2}$, the chirp parameter can be written:

$$\alpha \cong \alpha_0 \equiv \frac{A_1 + A_2}{A_1 - A_2} \qquad [5.152]$$

Under these conditions, if the electrodes are symmetric (A_1 = -A2) we obtain $\alpha_0 = 0$, and if the electric signal is applied to only one optical path (A_2 = 0) then $\alpha_0 = 1$.

Generally speaking, this parameter can affect the performances of optical transmissions because of the dispersion in optical fibers. Consequently, the management of the chirp according to the characteristics of the transmission line can considerably improve the performances and the capacity of the optical transmissions. An analysis of these effects can be found in [Cou 2002].

5.7. Modulation in optical networks: state-of-the-art

The evolution of data transmission using optical fiber has sped up since the appearance of the WDM (*wavelength demultiplexing multiplexing*) technique, which enables data to reach binary speeds of a few Tb/s transported by a single fiber. After having transmitted 2.5 Gb/s, then 10 Gb/s per channel on transmission lengths which reach hundreds of km, the need for high speed transmission (currently higher or equal to 40 Gb/s) on longer transmission lengths keeps growing. Figure 5.35 shows the evolution of the capacity per fiber from the 1980s until today.